Dalton Transactions

Fusion of photodynamic therapy and photoactivated chemotherapy: a novel Ru(II) arene complex with dual activities of photobinding and photocleavage toward DNA

Journal:	*Dalton Transactions*
Manuscript ID:	DT-ART-06-2014-001755.R2
Article Type:	Paper
Date Submitted by the Author:	12-Aug-2014

Complete List of Authors:	Chen, Yong-Jie; technical institute of physical chemistry, Lei, Wan-Hua Jiang, Guo-yu; technical institute of physical chemistry, Hou, Yuan-Jun li, chao; technical institute of physical chemistry, Zhang, Bao-Wen Zhou, Qian-Xiong Wang, Xuesong; Technical Institute of Physics and Chemistry,CAS ,

Cite this: DOI: 10.1039/c0xx00000x

www.rsc.org/xxxxxx

ARTICLE TYPE

Fusion of photodynamic therapy and photoactivated chemotherapy: a novel Ru(II) arene complex with dual activities of photobinding and photocleavage toward DNA

Yongjie Chen[a, b], Wanhua Lei[a], Guoyu Jiang[a], Yuanjun Hou[a], Chao Li[a], Baowen Zhang[a], Qianxiong Zhou*[a], Xuesong Wang*[a]

Received (in XXX, XXX) Xth XXXXXXXXX 20XX, Accepted Xth XXXXXXXXX 20XX
DOI: 10.1039/b000000x

The transition metal complexes with dual functions of DNA photobinding via coordination and DNA photocleavage via $^1O_2$ may present potent antitumor activities with high selectivity and wide anticancer spectrum. We reported herein a such complex, $[(\eta^6\text{-}p\text{-cymene})Ru(dpb)(py)]^{2+}$ (dpb = 2,3-bis(2-pyridyl)benzoquinoxaline, py = pyridine, **1**). The highly delocalized nature of dpb renders **1** a long wavelength-absorbing character and a long-lived excited state facilitating $^1O_2$ generation. Besides, the bulky feature of dpb leads to a distorted coordination geometry and allows for the ^{3}MC (metal-centered) state more accessible, from which dissociation of py and dpb may occur, followed by coordination of the resultant Ru fragment to nucleic bases if DNA is present. The dissociation of dpb can turn on the fluorescence of its own, enabling real-time imaging of the photoactivation process. The fascinating properties of **1** and the underlying mechanisms may provide guidelines for developing more efficient metallodrugs with dual potentials of photodynamic therapy (PDT) and photoactivated chemotherapy (PACT).

Introduction

In the combat against cancer over the past decades, the poor selectivity and specificity has been the bottleneck for chemotherapy, which accounts for the severe side effects of the clinical drugs. To hurdle this problem, two strategies are usually adopted in developing novel anticancer agents, *i.e.* selective delivery and selective activation. While the former approach tries to achieve preferential accumulation of drugs at diseased sites, the latter one makes drugs active only either upon exposure to the microenvironments specific to tumors, *e.g.* pH and redox potential, or in response to external stimulus, *e.g.* light, microwave, and alternating magnetic field.[1] Of these activation mechanisms, photoactivation is particularly unique. The facile delivery of illumination in a spatially and temporally controlled manner allows for on-demand drug dosing at desired location and time and therefore minimal impact to healthy tissues and cells.[2] As a type of photoactivation modality, photodynamic therapy (PDT) has got successful clinical application in treatment of many kinds of malignant and nonmalignant diseases.[3] In PDT, the spatially-confined irradiation of photosensitizer molecules and then the interaction of the excited photosensitizer molecules with oxygen and/or biomolecules generates cytotoxic reactive oxygen species (ROS), mainly singlet oxygen ($^1O_2$), leading to the death of cancer cells. One photosensitizer molecule can generate hundreds and thousands of $^1O_2$, partly accounting for the high efficiency of PDT. However, the oxygen-dependant character of PDT limits its efficacy toward hypoxic tumor cells.[4] In contrast, a new photoactivation modality emerging in recent years, *i.e.* photoactivated chemotherapy (PACT), has no such limitations. The PACT drug candidates developed currently are mainly transition metal complexes.[1a, 1b, 5] They generally show negligible or very low cytotoxicity in the dark. Once irradiated, they undergo ligand dissociation and the resultant metal complexes display anticancer activity by covalent binding to DNA or other cellular components in a manner similar to cisplatin,[6] a well-known first line clinical anticancer drug. Though PACT can work in both aerobic and anaerobic conditions, it generates active species stoichiometrically rather than catalytically as its counterpart of PDT. The high anticancer efficacy and broad anticancer spectrum may be achieved simultaneously by fusing PACT and PDT in one agent. Thus, the metallodrugs with dual PACT and PDT activities are appealing and warrant an extensive exploration for the pursuit of novel anticancer agents of high efficiency and selectivity. In this work, we reported on an intriguing Ru(II) arene complex, $[(\eta^6\text{-}p\text{-cymene})Ru(dpb)(py)]^{2+}$ (dpb = 2,3-bis(2-pyridyl)benzo quinoxaline, py = pyridine, complex **1** in Scheme 1), which is able to generate $^1O_2$ and undergo ligand dissociation upon visible light irradiation, showing dual potentials of PDT and PACT.

Ru(II) arene complexes of the type $[(\eta^6\text{-arene})Ru(X)(Y)(Z)]^{n+}$, in which X is a monodentate ligand (usually halide), Y and Z are monodentate or chelating ligands, are receiving increasing attention due to their unique anticancer activities, in particular toward cisplatin-resistant or metastasis tumors.[7] The anticancer activities of such type of complexes are highly associated with the labile nature of the X ligand. The replacement of X by pyridine or its derivatives may make the anticancer activity photoactivable. As an example, $[(\eta^6\text{-}p\text{-cymene})Ru(bpm)(py)]^{2+}$ (bpm = 2,2′-bipyrimidine, Scheme S1) undergoes ligand dissociation and DNA covalent binding upon irradiation with light around 400 nm, showing PACT activity.[8] Additionally, the replacement of X by a $^1O_2$ photosensitizer, such as porphyrin derivatives, endows the resultant complexes with PDT activity.[9-11] For clinical application, the photoactivation wavelength of Ru(II) arene complexes needs a red shift to the phototherapeutic window (650–900 nm) to achieve deeper tissue penetration.[12] In this regard, dpb drew our attention since its highly delocalized π system may shift ^{1}MLCT (metal-to-ligand charge transfer) absorption to lower energy.[13] Taking advantage of this property of dpb, we successfully constructed a series of new long wavelength-absorbing Ru(II) polypyridyl complexes, such as $[Ru(bpy)_{3-n}(dpb)_n]^{2+}$ and $[Ru(bpy)(dpb)(dppn)]^{2+}$ (bpy = 2,2'-bipyridine, dppn = 4,5,9,16-tetraaza-dibenzo[*a,c*]naphthacene, n = 1-3, Scheme S1), whose ^{1}MLCT absorption maxima (*ca.* 550 nm) have a red shift of 100 nm with respect to that of $[Ru(bpy)_3]^{2+}$ (450 nm).[14] Inspired by these results, we designed and synthesized $[(\eta^6\text{-}p\text{-cymene})Ru(dpb)(py)]^{2+}$ (**1**) with the aim to extend the photoactivation window to longer wavelengths. As expected, **1** indeed experiences ligand dissociation and covalent binding to DNA upon irradiation with light longer than 550 nm. However, out of our anticipation, **1** can also generate $^1O_2$ and photocleave DNA. Recently, Brewer and coworkers examined a series of binuclear transition metal complexes with a focus on their DNA binding and DNA cleavage.[15] Of which, $[(Ph_2phen)_2Ru(dpp)PtCl_2]^{2+}$ and $[(bpy)_2Os(dpp)RhCl_2(phen)]^{3+}$ (Ph_2phen = 4,7-diphenyl-1,10-phenanthroline, dpp = 2,3-bis(2-pyridyl)pyrazine), phen = 1,10- phenanthroline, Scheme S1) display DNA photobinding by the Pt or Rh moiety and DNA photocleavage by the Ru or Os moiety, respectively.[15a,b] To the best of our knowledge, **1** represents the first mononuclear Ru complex enabling DNA photobinding and photocleavage simultaneously. Additionally, we found that the ligand photodissociation of **1** occurs via not only monodentate py but also bidentate dpb, which restores the fluorescence of dpb and allows for optical imaging of the photoactivation process. To better understand the unprecedented photophysical, photochemical and photobiological properties of **1**, two structurally relevant complexes $[(\eta^6\text{-}p\text{-cymene})Ru(dpq)(py)]^{2+}$ and $[(\eta^6\text{-}p\text{-cymene})Ru(dpp)(py)]^{2+}$ (dpq = 2,3-bis-(2-pyridyl)-quinoxaline, complex **2** and **3** in Scheme 1) were also studied. The mechanisms behind the interesting photoactivation behavior of **1** may provide guidelines for the development of the multifunctional anticancer agents with PDT, PACT and imaging potentials.

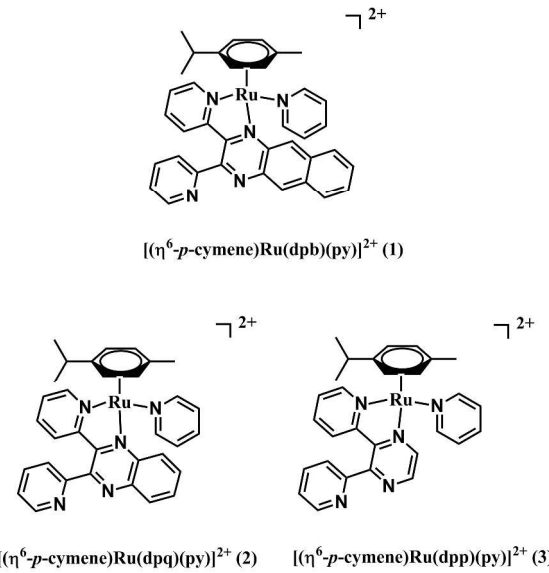

Scheme 1. Chemical structures of the examined Ru(II) arene complexes.

Results and discussion

Photophysical and electrochemical properties

Figure 1 shows the UV-vis absorption spectra of **1**, **2** and **3** in PBS buffer along with those of dpp, dpq and dpb. The peaks centered at 332 and 405 nm for **1**, 376 nm for **2**, and 330 nm for **3** may be attributed to the bidentate ligand-based transitions of dpb, dpq, and dpp, respectively. The red shift phenomena of bidentate ligand absorption band upon coordination to Ru(II) center were also found in our previously synthesized complexes. [14b]

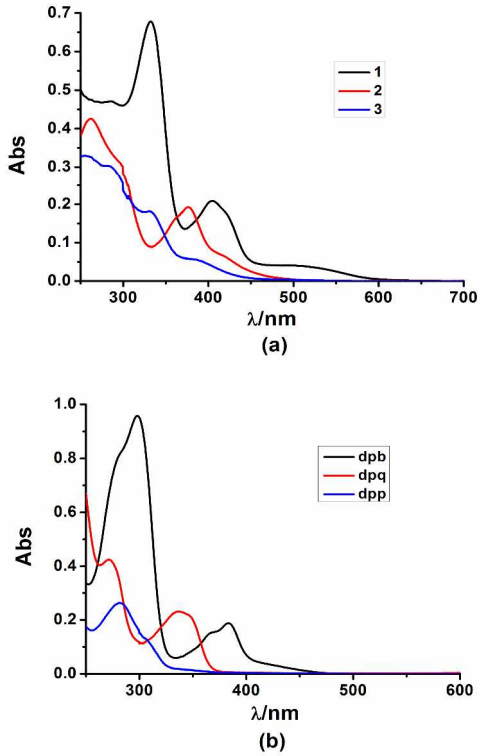

Figure 1. Absorption spectra of **1**, **2**, **3** (a) and dpp, dpq, dpb (b) in PBS (pH = 7.4, [solute] = 15 μM).

Table 1. Absorption maxima, reduction peak potentials, $^1O_2$ quantum yields and excited state lifetimes of the examined complexes.

Complex	Absorption maximum/nm[a]	E_p(red)[b]/V (*vs* SCE)	τ[b]/μs	$^1O_2$ quantum yields[b]
1	332, 405	-0.45	3.4	0.25
2	376	-0.51	--	--
3	330	-0.67	--	--

[a] In PBS buffer (pH 7.4). [b] In acetonitrile.

For Ru(II) arene complexes bearing a diimine ligand, the ^{1}MLCT transitions generally occur at around 400 nm.[8] Accordingly, the absorption band of **3** in the range of 360 – 460 nm may be attributed mainly to the dpp-based ^{1}MLCT transition. With the gradual enlargement of the delocalized π system from dpp to dpq to dpb, one may expect that the ^{1}MLCT transition will undergo a synchronized red shift as the result of the gradual decrease of the π* levels of these ligands. This is indeed what we observed, supporting our assignment very well. Notably, the ^{1}MLCT absorption of **1** stretches to 600 nm, appears to be the longest wavelength in the family of Ru(II) arene complexes examined so far.

In acetonitrile, dpp, dpq, and dpb showed reduction peak potentials ($E_{L(0/-1)}$) at -1.99, -1.63 and -1.34 V *vs* SCE, respectively. Upon coordination to Ru(II) center, their reduction peak potentials had a remarkable anodic shift, occurring at -0.45 V in **1**, -0.51 V in **2**, and -0.67 V in **3** (Table 1). Obviously, the π* levels of the bidentate ligands follow the order of dpb < dpq < dpp. In contrast, no Ru(+3/+2)-based redox processes were observed in cyclic voltammetry experiments of **1-3**. Similar electrochemical behavior was also found in [(η^6-*p*-cymene)Ru(bpy)(py)]$^{2+}$.[8a]

1-3 are non-emissive, a typical feature for the most Ru(II) arene complexes reported so far.[8] Among the three bidentate ligands, dpb is highly fluorescent with a quantum yield of 0.083 in PBS. The fluorescence loss of dpb upon coordination hints an efficient transition from ^{1}dpb* to ^{1}MLCT, in line with the lower energy of ^{1}dpb* than ^{1}MLCT.

Photoinduced ligand dissociation

The PBS solutions of **1-3** exhibited good stability in the dark as evidenced by negligible changes in their UV-vis absorption spectra after standing for 4 h (Figure S1-S3). In sharp contrast, visible light irradiation caused remarkable variations in the absorption spectra of these complexes. As shown in Figure 2b, spectrum changes of **3** led to three isosbestic points, indicative of the formation of a new species, which is most likely due to the photodissociation of the monodentate ligand py. This was confirmed by high resolution ESI MS (Figure S4). Irradiation gave a new signal at m/z = 487.10655, assignable to [(η^6-*p*-cymene)Ru(dpp)(OH)]$^+$ due to the exchange of py with water. In the presence of 9-ethylguanine (9-EtG), the signal of [(η^6-*p*-cymene)Ru(dpp)(9-EtG)]$^{2+}$[PF$_6$]$^-$ (m/z = 794.15070) was observed (Figure S5), vindicating the photodissociation of py and demonstrating the coordination potential of the resultant Ru(II) arene fragment toward nucleic bases. Additionally, the ^{1}H NMR spectrum changes of **3** (Figure S6) provided further evidence for ligand dissociation, though the signals of free py ligand were buried in that of **3**. The irradiation of **2** led to similar changes in UV-vis absorption spectrum and MS (Figure 2a and Figure S7). Particularly, the chemical shifts of free py ligand were identified clearly upon irradiation of **2** (Figure S8), suggesting an identical photochemical reaction, *i.e.* the monodentate ligand dissociation, took place.

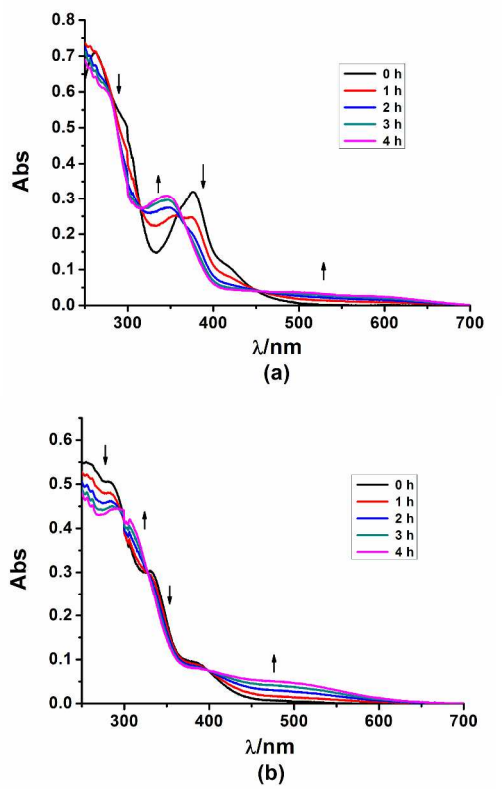

Figure 2. Absorption spectra changes of **2** (a) and **3** (b) in PBS (pH = 7.4, [**2**] = [**3**] = 25 μM) upon irradiation with λ > 400 nm.

1 behaved in a somewhat different manner when irradiated with λ > 400 nm (Figure 3, S9 and S10). Unlike **2** and **3**, no isosbestic points were observed in the absorption spectra of **1** throughout the irradiation, suggesting that there were at least two types of new species formed, Figure 3. Moreover, the irradiation in the presence of 9-EtG gave two new m/z signals (Figure S9) at 894.18021 and 335.12889, assignable to [(η^6-*p*-cymene)Ru(dpb)(9-EtG)]$^{2+}$[PF$_6$]$^-$ and [dpb + H]$^+$, respectively. This result indicates that both py and dpb dissociated from the Ru center upon irradiation. The photodissociation of dpb is unambiguously confirmed by fluorescence measurement, Figure 4. The irradiation led to partial restoration of the dpb fluorescence, whereas the bound dpb is totally nonemissive. Irradiation also resulted in significant changes in ^{1}H NMR spectrum of **1** (Figure S10). In this case, the signals of both free py and dpb were observed. In particular, the chemical shifts of the two protons (H$_a$ and H$_b$, inset of Figure S10) of the central ring of benzoquinoxaline showed remarkable changes in free dpb, **1**, and the py-leaving product. Based on this, the ratio of the py-leaving and dpb-leaving products was estimated to be 3.4:1. We also monitored the ^{1}H NMR spectra of **1** upon irradiation in the presence of excess 9-EtG (Figure S11). Interestingly, the dpb-

leaving product became predominant in this condition. Several new resonant peaks that were not present in Figure S10 were observed, which may be attributed to the 9-EtG substituted products (see details in ESI). The ligand dissociation rate of **1** in CD_3COCD_3/D_2O was found to be much lower than that in PBS, indicating the role of solvent. Notably, the ligand dissociation of **1** proceeded efficiently upon irradiation with light > 550 nm (Figure S12), obviously benefited from the long wavelength-absorbing feature of **1**.

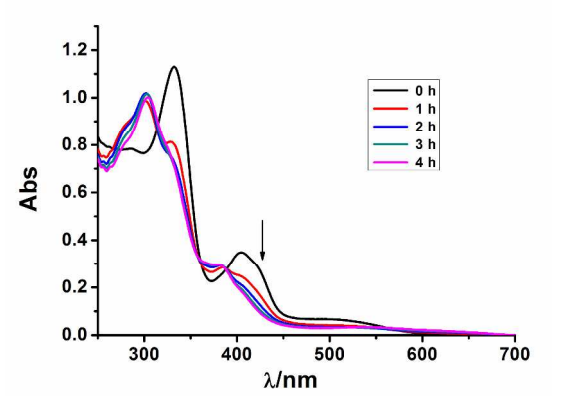

Figure 3. Absorption spectra changes of **1** (25 μM) in PBS (pH = 7.4) upon irradiation with λ > 400 nm.

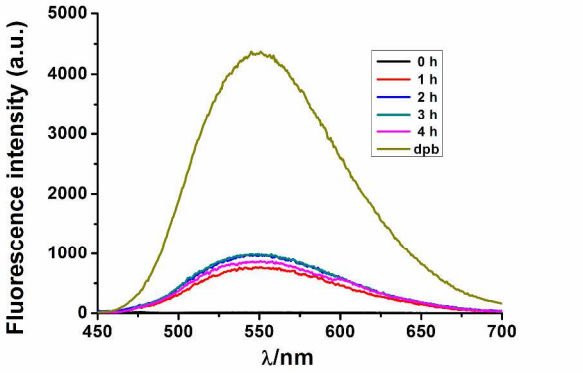

Figure 4. Fluorescence spectra changes of **1** (25 μM) in PBS (pH = 7.4) upon irradiation with λ > 400 nm.

Though bidentate ligands are not prone to dissociation due to their chelation ability, sterically hindered bidentate ligands may become photo-labile in some cases. Recently, E. C. Glazer reported a series of such kind of Ru(II) complexes, *e.g.* $[Ru(bpy)_2(6,6'\text{-dimethyl-}2,2'\text{-bpy})]^{2+}$ and $[Ru(bpy)_2(2,9\text{-dimethyl-dipyrido}[3,2\text{-}f\text{:}2',3'\text{-}h]\text{ quinoxaline})]^{2+}$ (Scheme S1), in which dimethyl-substitued bidentate ligands can dissociate efficiently when irradiated.[5b] The underlying mechanism is that the sterically hindered ligand distorts the coordination geometry and decreases the energy of the metal-centered (^{3}MC) state, accordingly making ^{3}MC, a state responsible for ligand dissociation,[16] more thermally accessible from ^{3}MLCT. This mechanism may play a role in the case of **1**. We noticed that the two methyls on the isopropyl group of *p*-cymene of **1-3** are not magnetically equivalent as evidenced by a double doublet pattern in their ^{1}H NMR spectra (Figure S13-15). In sharp contrast, only one doublet was observed in our previously reported complexes, such as $[(\eta^6\text{-}p\text{-cymene})Ru(dppn)(py)]^{2+}$, $[(\eta^6\text{-}p\text{-cymene})Ru(dppz)(py)]^{2+}$, and $[(\eta^6\text{-}p\text{-cymene})Ru(phen)(py)]^{2+}$ (dppz = dipyrido[3,2-*a*:2',3'-*c*]phenazine], see their chemical structures in Scheme S1).[17] The splitting of the two methyl groups indicates that the isopropyl group in **1-3** cannot rotate freely in solutions, probably due to the steric hindrance rendered by dpb, dpq, and dpp. Interestingly, the splitting (the distance between both doublet) becomes more and more significant from 0.025 ppm for **3** to 0.08 ppm for **2** to 0.11 ppm for **1**, in hint of an increasing steric hindrance from **3** to **1**.

We luckily obtained single crystals of **2** that are suitable for X-ray diffraction analysis, from which more clues on ligand steric effect may be obtained (Figure 5, Table 2 and S1, CCDC 988455). As shown in Figure 5, the isopropyl group locates on top of dpq with C34-C33 bond parallel with dpq, C34-C32 bond pointing far away from dpq, and C34-H bond directing toward dpq. This may be the least strained conformation available for **2** in the solid state. In solution, the rotation of the isopropyl group around C34-C27 bond will have to pass a high strain state in which one methyl group extrudes toward dpq. Consequently, the hindered rotation makes the two methyl groups no longer magnetically equivalent. Additionally, the bond lengths of Ru1-N1 and Ru1-N3 are 2.135 and 2.072 Å, respectively (Table 2). In contrast, the corresponding bond lengths of many Ru(II) arene complexes are in the range of 2.06-2.08 Å.[18] Specifically, the bond lengths of Ru-N(dpq) in $[(\eta^6\text{-}p\text{-cymene})Ru(dpq)(Cl)]^+$ are 2.059 and 2.089 Å, respectively, [18c] suggesting that the remarkably lengthened Ru1-N1 in **2** results from the repulsion of dpq and py. The coordination distorsion may be more significant in **1**, rendering dpb labile.

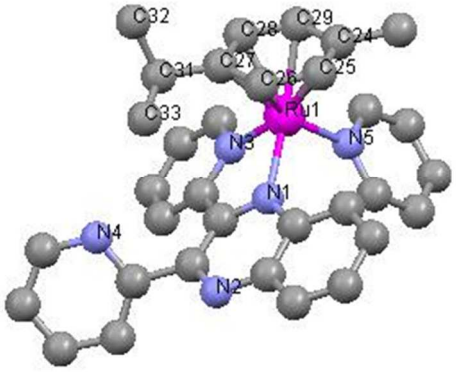

Figure 5. Crystal structure of **2** with thermal ellipsoids at 50% probability (PF_6^-, CH_3CN and hydrogen atoms have been omitted for clarity).

Table 2. Selected bond lengths and angles for **2**.

Bond distance (Å)		Bond angles (°)	
Ru(1)-N(3)	2.072(5)	N(3)-Ru(1)-N(5)	84.6(2)
Ru(1)-N(5)	2.131(6)	N(3)-Ru(1)-N(1)	76.2(2)
Ru(1)-N(1)	2.135(6)	N(5)-Ru(1)-N(1)	92.6(2)
Ru(1)-C(28)	2.185(6)		
Ru(1)-C(26)	2.202(6)		
Ru(1)-C(29)	2.203(6)		
Ru(1)-C(25)	2.226(6)		
Ru(1)-C(27)	2.232(6)		
Ru(1)-C(24)	2.276(7)		

$^1O_2$ generation

The photodissociation of dpb prompted us to examine the $^1O_2$ generation ability of **1,** because free dpb is able to produce $^1O_2$ via its triplet excited state. To our surprise, **1** can generate $^1O_2$ on its own.

We at first carried out EPR experiments of **1** in CH_3CN in the presence of TEMP, a well known spin trapping agent of $^1O_2$.[19] Upon irradiation with 532 nm laser, a three-line signal with a hyperfine coupling constant of 16.0 G, attributable to the adduct of $^1O_2$ and TEMP, *i.e.* TEMPO, was observed (Figure 6). The control experiments revealed that both irradiation and oxygen are necessary for the appearance of the signal. Additionally, the addition of NaN_3, a common scavenger of $^1O_2$,[20] restricted the signal greatly, confirming the assignment of TEMPO further. We also examined the absorption and emission spectra of **1** in CH_3CN before and after irradiation at $\lambda > 400$ nm for 4 h to assess the ligand photodissociation. To our surprise, negligible ligand photodissociation was observed in CH_3CN solution (Figure S16), indicating again that the ligand photodissociation of **1** is highly solvent-dependant. The result also suggests that $^1O_2$ generated in EPR experiments originated from **1** itself. In contrast, no TEMPO signals were found in the cases of **2** and **3** irrespective of the irradiation wavelength (532 or 355 nm).

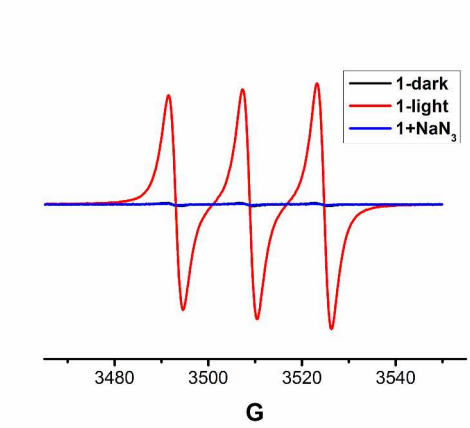

Figure 6. EPR signals obtained upon irradiation of O_2-saturated CH_3CN solutions of 50 mM TEMP and 0.5 mM **1** with 532 nm laser. Dark control means without light irradiation.

The $^1O_2$ quantum yields of **1-3** in CH_3CN were quantitatively measured using $[Ru(bpy)_3]^{2+}$ as the standard (Φ_Δ = 0.57 in CH_3CN[21]) and DPBF as the trapping agent.[22] DPBF can react efficiently with $^1O_2$ to form endoperoxide product, a process that may be followed easily by either absorption or fluorescence spectrum. We found that DPBF itself underwent photo-bleaching when irradiated at 400 nm. Taking this into consideration, the $^1O_2$ quantum yield of **1** was measured to be 0.25, while that of **2** and **3** are too low to be measured (Table 1). In the same condition, dpb has a $^1O_2$ yield of 0.34.

We also examined the $^1O_2$ generation abilities of **1-3** in PBS buffer. As shown in Figure 7a, irradiation at 400 nm led to the bleaching of DPBF. The addition of **2** or **3** did not accelerate DPBF bleaching, in line with their poor $^1O_2$ generation ability. In the presence of **1**, the bleaching rate of DPBF was improved greatly, demonstrating that **1** is still able to generate $^1O_2$ in aqueous solution. Due to the ligand photodissociation in PBS buffer, the released dpb ligand may make some contribution in $^1O_2$ generation. When irradiated at 550 nm (Figure 7b), DPBF showed strong stability since it cannot absorb the light of this wavelength. Accordingly, the photoinduced DPBF bleaching may be exclusively attributed to $^1O_2$ generated by **1**. In this case, the contribution from free dpb can be rule out due its negligible absorbance at 550 nm.

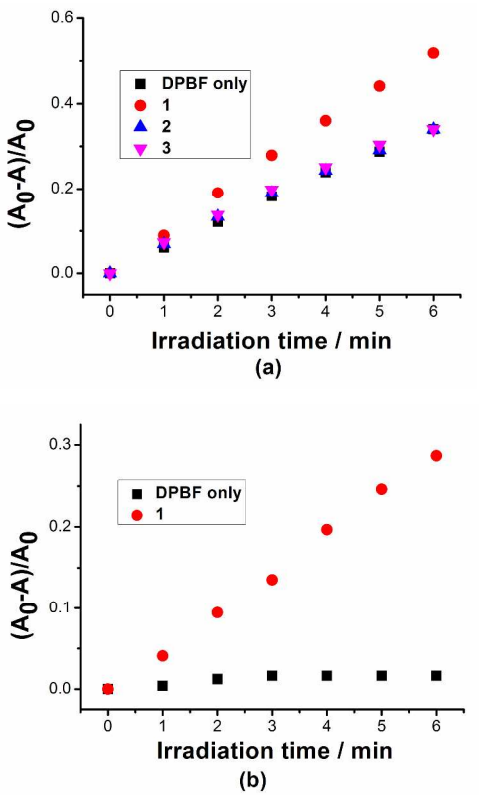

Figure 7. DPBF bleaching (at 405 nm) in the presence of **1**, **2** or **3** in PBS (pH = 7.4, [DPBF] = 12 μM) upon irradiation at 400 nm (a) or 550 nm (b).

To reasonably explain the $^1O_2$ yields of **1-3**, we measured their transient absorption spectra in Ar-saturated CH_3CN. No any signals were observed upon irradiation of **2** or **3** using 355 nm laser, in line with short-lived ^{3}MLCT as the lowest energy excited states of Ru(II) arene complexes. For **1**, irradiation gave transient absorption spectra with the lifetime as long as 3.4 μs (Figure 8a), correlating very well with its good $^1O_2$ yield. The transient absorption spectra of **1** and dpb (Figure 8b) exhibit a valley at 420 nm and 360 nm respectively, corresponding to their ground state absorption maxima at 405 nm and 383 nm (Figure 1) very well. Additionally, the fluorescence emission of dpb may account for the low ΔOD of dpb beyond 550 nm. Taking these factors into consideration, the transient absorption spectra of **1** are very similar to that of dpb in both spectrum profile and decay kinetics (lifetime of 4.0 μs for ^{3}dpb*). Thus, the lowest energy excited state of **1** may mainly localize at ^{3}dpb*. In this aspect, **1** is reminiscent of $[(\eta^6\text{-}p\text{-cymene})Ru(dppn)(py)]^{2+}$ (Scheme S1), whose lowest energy excited state populates at ^{3}dppn* and therefore exhibits a long-lived transient absorption spectrum similar to that of free dppn ligand.[17] Similar to **1**, $[(\eta^6\text{-}p\text{-cymene})Ru(dppn)(py)]^{2+}$ can generate $^1O_2$ with a quantum yield

of 0.22 in CH_3CN.[17]

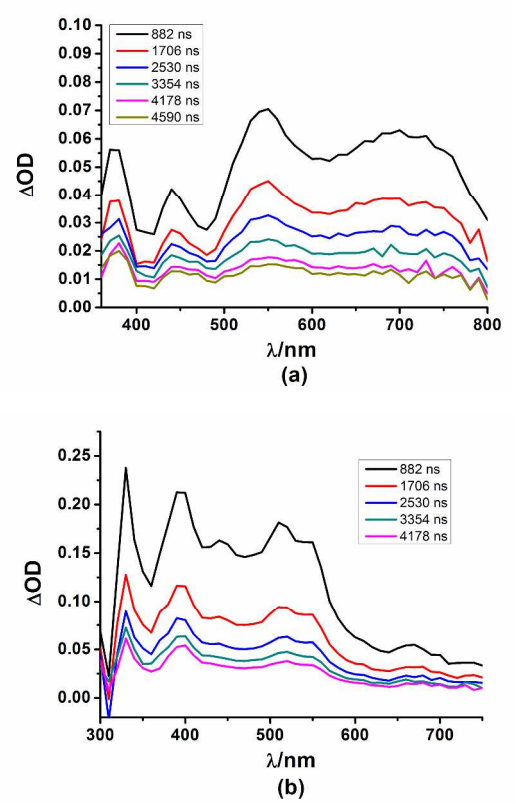

Figure 8. Transient absorption spectra of **1** (a) and dpb (b) in Ar-saturated CH_3CN solutions upon pulsed excitation at 355 nm.

Bearing in mind all aforementioned results and discussion, we tentatively put forth a possible energy level diagram of **1.** As shown in Scheme 2, the relative energies of the photoactivation-pertinent excited states should follow the order of $^1dpb^*$ > ^{1}MLCT > ^{3}MLCT > $^3dpb^*$. The relative position of ^{3}MC is uncertain yet, however, it should be in proximity in energy to ^{3}MLCT and/or $^3dpb^*$. There are two key factors involved in this diagram. The first one lies in the long-lived lowest energy excited state of $^3dpb^*$, which renders **1** $^1O_2$ generation capability. The other one stems from the steric hindrance effect of dpb, which lowers the energy of ^{3}MC and facilitates ligand photodissociation. For **2** and **3**, the lowest excited triplet state is ^{3}MLCT, which is

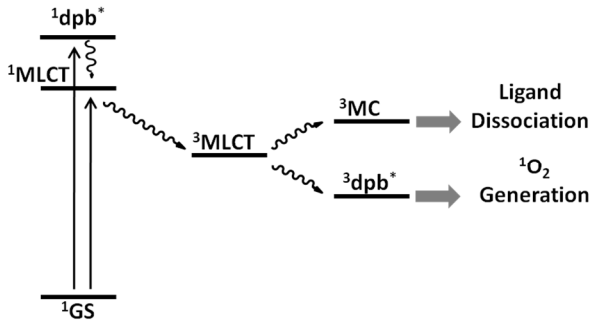

Scheme 2. Possible energy level diagram for **1**.

short lived and therefore has no chance to undergo intermolecular interaction with O_2 to generate $^1O_2$. Thus, the ^{3}MLCT state of **2** or **3** will either decay via ^{3}MC to lead to ligand dissociation or decay directly to the ground state. **1** is expected to photobind DNA in anaerobic condition via ligand dissociation mechanism and to interact with DNA by both photobinding and photocleavage in aerobic environment. Importantly, the two effects in later case are cumulative, *i.e.* **1** may generate $^1O_2$ catalytically until it undergoes ligand dissociation and then serves as a DNA binding agent.

Photobinding and photocleavage toward DNA

The photoinduced DNA damage abilities of **1-3** were compared by agarose gel electrophoresis using supercoiled pUC19 DNA as target. Figure 9 shows the electrophoresis pattern of the supercoiled pUC19 DNA irradiated for 40 min at λ > 400 nm in different conditions. Irradiation alone did not damage DNA, Lane 3. However, the migration of the supercoiled circular (SC) DNA reduced markedly upon irradiation in the presence of **3,** Lane 2. Meanwhile, the fluorescence intensity of the SC band decreased as well. Both phenomena may be due to the photoinduced covalent binding of **3** to DNA, which on one hand alters the tertiary structure, apparent molecular weight and net charges of DNA and accordingly the mobility rate, and on the other hand restricts the intercalation of EB and therefore the fluorescence intensity.[15] Similar results were also obtained upon irradiation of the DNA samples in the presence of **1** or **2** (Lane 5 and 7), and the photobinding efficiencies of the three complexes follow the order of **1** > **3** >> **2**. In the dark, **1-3** did not change the mobility of SC (Lane 1, 4, and 6), confirming that the DNA binding results from irradiation. The DNA photobinding of such type of Ru complexes are generally believed to begin with the ligand photodissociation, followed by coordination of the resultant Ru fragment to nucleic bases. The red shifted absorption spectrum in combination with the bidentate ligand dissociation may facilitate the photobinding of **1** greatly.

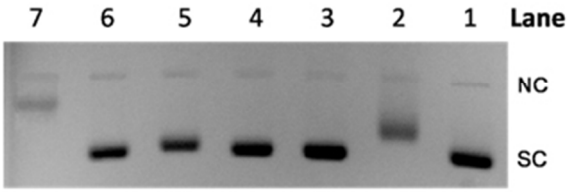

Figure 9. Agarose gel electrophoresis pattern of supercoiled pUC19 DNA (40 μg/mL) in air-saturated Tris-CH_3COOH/EDTA buffer (pH = 7.4) in different conditions. Lane 1, DNA + **3** (dark); Lane 2, DNA + **3** (light); Lane 3, DNA alone (light); Lane 4, DNA + **2** (dark); Lane 5, DNA + **2** (light); Lane 6, DNA + **1** (dark); Lane 7, DNA + **1** (light). [**1**] = [**2**] = [**3**] = 50 μM, dark refers to without irradiation, light refers to irradiation at λ > 400 nm for 40 min. SC and NC denote supercoiled circular and nicked circular forms, respectively.

For more intensive comparison, the mobility shift assay was carried out in both aerobic and anaerobic conditions and in the presence of varied concentrations of **1** and **3** (Figure 10 and 11). As shown in Figure 10, both **1** and **3** show a dose-dependent photobinding behavior and **1** photobinds DNA far more potently than **3** in the same concentration. Interestingly, in the presence of

10 μM of **1**, the reduced mobility and enhanced fluorescence intensity were observed at the same time for the nicked circular (NC) DNA (Figure 10, Lane 5). The result is producible and may be explained as the synergistic effect of photobinding and photocleavage. The photobinding of **1** toward SC and NC retards their mobility and weakens their fluorescence intensity, while the photocleavage of **1** toward SC diminishes the fluorescence intensity of SC but increase the fluorescence intensity of NC, since the cleavage of SC leads to the formation of NC. Thus, the opposite effects of the photobinding and photocleavage on the fluorescence intensity of NC may allow for the resolution of both mechanisms in proper conditions, just like the case of Lane 5. Though photocleavage is not discernible in the lane 6 and 7, one may expect that it should make a contribution to the so efficient bleaching of the SC band in both cases.

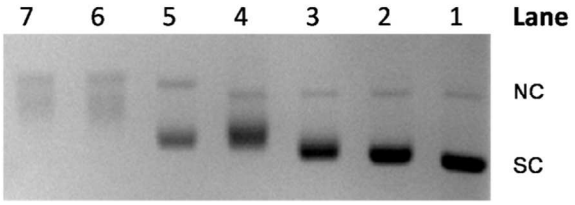

Figure 10. Agarose gel electrophoresis pattern of supercoiled pUC19 DNA (40 μg/mL) in air-saturated Tris-CH_3COOH/EDTA buffer (pH = 7.4) irradiated at λ > 400 nm for 40 min in the presence of varied concentrations of **1** or **3**. Lane 1: DNA alone; Lanes 2-4: 10, 25, and 50 μM of **3**; Lanes 5-7: 10, 25, and 50 μM of **1**. SC and NC denote supercoiled circular and nicked circular forms, respectively.

The DNA photocleavage of **1** most likely relies on its $^1O_2$ generation ability. This is why the enhanced NC band is no longer observable in Ar-saturated solutions, irrespective of the concentration of **1** (Lane 5-7, Figure 11). Under Ar atmosphere, the photobinding is still in effect for **1.** However, the bleaching of the SC band appears less efficient than that in air-saturated condition (Figure 10 *vs* Figure 11), suggesting that the efficient SC bleaching observed in the lane 5-7 of Figure 10 is indeed the result of the combination of photobinding and photocleavage. **3** behaved similarly in both aerobic and anaerobic conditions (lane 2-4 in Figure 10 *vs* lane 2-4 in Figure 11), in line with the single photobinding potential of **3**.

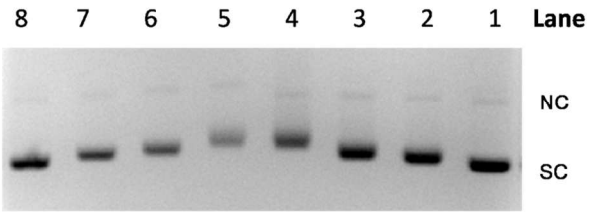

Figure 11. Agarose gel electrophoresis pattern of supercoiled pUC19 DNA (40 μg/mL) in Ar-saturated Tris-CH_3COOH/EDTA buffer (pH = 7.4) irradiated at λ > 400 nm for 40 min in the presence of varied concentrations of **1** or **3**. Lane 1 and 8: DNA alone; Lanes 2-4: 10, 25, and 50 μM of **3**; Lanes 7-5: 10, 25, 50 μM of **1**. SC and NC denote supercoiled circular and nicked circular forms, respectively.

To explore further the role of $^1O_2$, we studied the effects of NaN_3, DABCO and Ar on the photodamage of **1** toward DNA (Figure 12). In Figure 12, the irradiation time employed was 30 min. In this condition, the NC band with reduced mobility but enhanced fluorescence intensity was observed again (Lane 4), displaying further the cooperation between the photobinding and photocleavage of **1**. In Ar atmosphere (Lane 2), the mobility slowing for both SC and NC was still visible, however, the intensity of the NC band was not improved, in line with the loss of $^1O_2$ mechanism. In air-saturated solutions and in the presence of DABCO (Lane 3) or NaN_3 (Lane 5), both are efficient scavengers of $^1O_2$,[20] not only photocleavage but also photobinding was significantly inhibited. While the inhibition on photocleavage is anticipated, the inhibition on photobinding is quite strange. We then examined the influences of DABCO and NaN_3 on the photodissociation of **1**. As shown in Figure S17, the absorption spectrum of **1** varied in a manner similar to Figure 3a upon irradiation at λ > 400 nm for 4 h in the presence of DABCO or NaN_3. However, the spectrum of the resultant solution is significantly different with that obtained by irradiation of **1** alone for 4 h and then addition of the same amount of DABCO or NaN_3. This finding implies that ligand exchange with DABCO or NaN_3 may occur during irradiation, which will block the ligand exchange between the labile ligands and nucleic bases. As a result, both photobinding and photocleavage of **1** were restricted by DABCO and NaN_3.

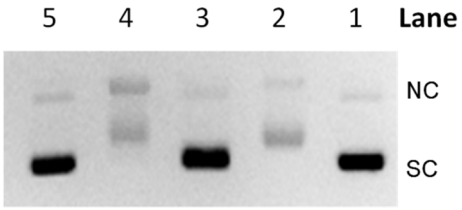

Figure 12. Agarose gel electrophoresis pattern of supercoiled pUC19 DNA (40 μg/mL) in Tris-CH_3COOH/EDTA buffer (pH = 7.4) irradiated at λ > 400 nm for 30 min in the presence of **1** (50 μM). Lane 1, dark control; Lane 2, Ar atmosphere; Lane 3, DABCO (50 mM); Lane 4, air atmosphere; Lane 5, NaN_3 (50 mM). SC and NC denote supercoiled circular and nicked circular forms, respectively.

The integration of DNA photobinding via coordination and DNA photocleavage via $^1O_2$ in a single agent may offer the system dual potentials of PACT and PDT. Brewer and coworkers recently constructed two binuclear complexes, $[(Ph_2phen)_2Ru(dpp)PtCl_2]^{2+}$ and $[(bpy)_2Os(dpp)RhCl_2(phen)]^{3+}$ (Scheme S1), that display DNA photobinding and DNA photocleavage simultaneously.[15a,b] They also reported many binuclear complexes that have DNA photocleavage and DNA thermal binding properties.[15c,d] To our best knowledge, **1** represents the first example to combine both DNA photobinding and DNA photocleavage in a mononuclear Ru(II) arene complex. Notably, the dual functions still work very well under irradiation at λ > 550 nm (Figure S12, Figure 7b and Figure S18) due to the long wavelength absorbing property of **1**.

Phototoxicity

The DNA photodamage activities of **1**, **2** and **3** prompted us to

examine their *in vitro* antitumor potentials under visible light irradiation (λ > 400 nm) using the human lung carcinoma cells A549 as target. Cells were incubated with the complexes for 4 h in the dark, then irradiated for 1 h, and incubated for another 20 h in the dark. Cell survival was quantified by way of MTT assay (Figure 13). Only **1** showed a significant light-enhanced cytotoxicity, with IC_{50} of 27.6 and 4.0 μM in the dark and under illumination, respectively. In sharp contrast, both **2** and **3** exhibited negligible phototoxicity. Because the three complexes show comparable ligand dissociation rates, the unique phototoxicity of **1** might associate with its $^1O_2$ generation and bidentate ligand dissociation. Many factors may exert large effects on the photophysical and photochemical properties and thus the phototoxicity of a drug candidate, including cellular uptake, subcellular localization, microenvironments (*e.g.* pH, polarity, O_2 concentration), as well as supramolecular interactions with bioactive components (*e.g.* DNA, RNA, protein, enzyme, polypeptide, lipid). The true reasons behind the large disparity in the phototoxicity of **1-3** remain elusive, however, the preliminary *in vitro* experiments indeed show the application potential of **1** as photoactivated antitumor drug candidate.

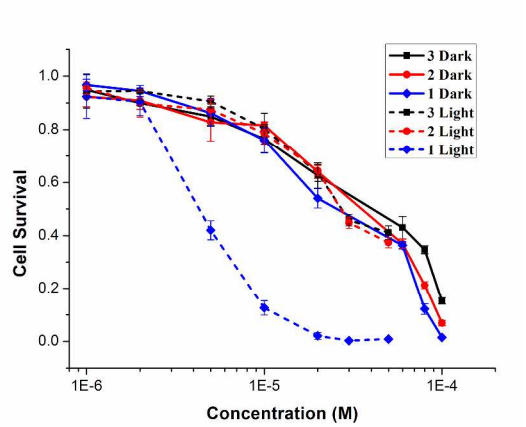

Figure 13. Cytotoxicity of **1-3** against A549 cells in the dark or under irradiation (λ > 400 nm) for 1 h.

Though **1** is nonemissive, the photodissociation of dpb can partially restore the fluorescence, making the real-time imaging possible in live cells. Figure S19 shows the confocal micrographs of the double-stained A549 (human lung carcinoma) cells with Hoechst 34580 (a nucleus-specific fluorescent probe) and **1.** Without pre-illumination, only blue fluorescence from Hoechst 34580 was observed. After irradiation at λ > 400 nm for 30 min, the fluorescence from both Hoechst 34580 and dpb were detected through blue and red channels, respectively, demonstrating that the dpb photodissociation took place effectively in cellular environment. The perfect superposition of blue and red fluorescence suggests that **1** and/or the released dpb accumulate selectively in the nucleus region.

Conclusions

Three Ru(II) arene complexes **1-3** were compared in detail on their photophysical, photochemical, and photobiological properties. While **2** and **3** undergo monodentate ligand dissociation upon irradiation, the photodissociation of both monodentate and bidentate ligands can occur in **1**. Moreover, **1** is able to generate $^1O_2$ on its own but **2** and **3** are not. As a result, **2** and **3** are only active in DNA photobinding. In contrast, **1** has both DNA photobinding and DNA photocleavage abilities, and therefore application potential as the new type of antitumor agents with dualmodal photoactivation mechanisms, *i.e.* PACT and PDT. Besides, the dissociation of dpb from **1** allows for real-time fluorescence imaging of the photoactivation process. Additionally, the photoactivation wavelength of **1** is much longer than that of **2** and **3**, extending nearly into the phototherapeutic window. These unique properties of **1** may stem from the bulky and highly delocalized dpb ligand. The bulky feature of dpb makes **1** in a strained coordination sphere and accordingly decreases the ligand field splitting energy and makes ^{3}MC (a state responsible for ligand dissociation) more thermally accessible. One the other hand, the highly delocalized nature of dpb makes the long-lived ^{3}dpb* become the lowest energy excited state and thus offers **1** the ability to generate $^1O_2$. The fascinating properties of **1** and the underlying mechanisms may provide guidelines for developing more efficient metallodrugs with dual potentials of PDT and PACT.

Experimental Section

Materials

2,3-Bis-(2-pyridyl)-pyrazine (dpp), 2,3-diaminonaphthalene, o-phenylenediamine, 2,2'-pyridil, pyridine, $[(p\text{-cymene})RuCl_2]_2$, NH_4PF_6, $AgNO_3$, ethidium bromide (EB), 1,3-diphenylisobenzofuran (DPBF), 2,2,6,6-tetramethyl-4-piperidone (TEMP), sodium azide (NaN_3), gel loading buffer, tris-hydroxymethyl-aminomethane (Tris base), tetra-*n*-butylammonium hexafluorophosphate, ethylenediaminotetracetic acid (EDTA), 1,4-diazabicyclo[2.2.2]octane (DABCO) were purchased from Sigma-Aldrich. Hoechst 34580 and supercoiled pUC19 plasmid DNA were obtained from Invitrogen and TaKaRaBiotechology, respectively. The PBS buffer solutions of **1-3** were prepared by diluting the stock solution of **1-3** in DMSO (1 mM) with proper volume of PBS, making the final volume ratio of DMSO not more than 5%.

Synthesis

The ligands dpb and dpq were synthesized following the reported method.[23] The complexes **1**, **2** and **3** were prepared following a published method.[8a,17] Taking **3** as an example, 122.5 mg $[(p\text{-cymene})RuCl_2]_2$ and 93.7 mg dpp were refluxed in 10 mL methanol for 4 h. After cooling to room temperature, 10 mL of $AgNO_3$ (136 mg) aqueous solution was added. After reflux for 3 h, the reaction solution was filtered. The filtrate was then refluxed again for 4 h, with pyridine (4 equiv) added. The whole reactions were conducted under N_2 atmosphere. After removal of solvent, the solid was purified by column chromatography on silica gel using $CH_3CN/H_2O/KNO_3$ (40:4:1) as eluent. The obtained compound was dissolved in methanol/water (1:1) and precipitated by NH_4PF_6, and the yellow solid was filtered, washed with water and dried under vacuum. Yield, 70%. The synthetic methods of **1** and **2** were similar to that of **3**, using dpb or dpq instead of dpp.

[(η^6-*p*-cymene)Ru(dpb)(py)](PF_6)$_2$ (1). ^{1}H NMR (400 MHz, in CD_3CN): δ = 0.90 (d, 3H, *J* = 6.9 Hz), 1.02 (d, 3H, *J* = 6.9 Hz), 2.24 (s, 3H), 2.43-2.50 (m, 1H), 6.13 (d, 1H, *J* = 6.2 Hz), 6.19 (d,

1H, *J* = 5.3 Hz), 6.46 (d, 1H, *J* = 6.3 Hz), 6.60 (d, 1H, *J* = 5.4 Hz), 7.23 (d, 1H, *J* = 9.0 Hz), 7.27-7.31 (m, 2H), 7.61-7.65 (m, 1H), 7.73-7.76 (m, 1H), 7.81-7.95 (m, 4H), 8.16-8.21 (m, 1H), 8.29-8.31 (m, 3H), 9.42-9.44 (m, 1H), 9.53-9.55 (m, 2H), 9.11 (s, 1H), 9.18 (s, 1H), 9.50 (d, 1H, *J* = 5.6 Hz). ESI-MS: m/z = 324.58851 $(M\text{-}2PF_6)^{2+}$, 794.14271 $(M\text{-}PF_6)^{+}$. Anal. Calcd for $C_{37}H_{33}F_{12}N_5P_2Ru\cdot 1.5H_2O$: C, 46.02; H, 3.76; N, 7.25. Found: C, 46.00; H, 3.77; N, 7.26.

[(η^6-*p*-cymene)Ru(dpq)(py)](PF_6)$_2$ (2). ^{1}H NMR (400 MHz, in CD_3CN): δ = 0.89 (d, 3H, *J* = 6.9 Hz), 0.97 (d, 3H, *J* = 6.9 Hz), 2.13 (s, 3H), 2.39-2.46 (m, 1H), 6.07 (t, 2H, *J* = 5.7 Hz), 6.33 (d, 1H, *J* = 6.2 Hz), 6.54 (d, 1H, *J* = 6.5 Hz), 7.19 (d, 1H, *J* = 8.1 Hz), 7.33 (t, 2H, *J* = 7.4 Hz), 7.61-7.65 (m, 1H), 7.71-7.75 (m, 1H), 7.83 (t, 1H, *J* = 7.9 Hz), 7.90 (t, 1H, *J* = 7.7 Hz), 8.14-8.34 (m, 6H), 8.43-8.46(m, 1H), 8.54(d, 1H, *J* = 4.6 Hz), 8.62(d, 1H, *J* = 8.1 Hz), 9.45(d, 1H, *J* = 5.6 Hz). HR ESI-MS: m/z = 299.57961 $(M\text{-}2PF_6)^{2+}$, 744.12161 $(M\text{-}PF_6)^{+}$. Anal. Calcd for $C_{33}H_{31}F_{12}N_5P_2Ru\cdot 0.5H_2O$: C, 44.16; H, 3.59; N, 7.80. Found: C, 44.15; H, 3.61; N, 7.79.

[(η^6-*p*-cymene)Ru(dpp)(py)](PF_6)$_2$ (3). ^{1}H NMR (400 MHz, in CD_3CN): δ = 0.94 (d, 3H, *J* = 6.9 Hz), 0.97 (d, 3H, *J* = 6.9 Hz), 1.83 (s, 3H), 2.48-2.55 (m, 1H), 6.02 (d, 1H, *J* = 6.4 Hz), 6.06 (d, 1H, *J* = 6.3 Hz), 6.32 (d, 1H, *J* = 6.4 Hz), 6.39 (d, 1H, *J* = 6.4 Hz), 7.02 (d, 1H, *J* = 7.2 Hz), 7.41-7.45 (m, 2H), 7.56-7.60 (m, 1H), 7.79-7.89 (m, 3H), 7.94 (t, 1H, *J* = 7.7 Hz), 8.05-8.09 (m, 1H), 8.33 (d, 2H, *J* = 5.2 Hz), 8.48 (d, 1H, *J* = 4.7 Hz), 9.06 (d, 1H, *J* = 3.0 Hz) , 9.58-9.61 (m, 2H). HR ESI-MS: m/z = 274.57280 $(M\text{-}2PF_6)^{2+}$, 694.11167 $(M\text{-}PF_6)^{+}$. Anal. Calcd for $C_{29}H_{29}F_{12}N_5P_2Ru\cdot H_2O$: C, 40.66; H, 3.65; N, 8.18. Found: C, 40.64; H, 3.66; N, 8.17.

Acknowledgements

This work was financially supported by the Ministry of Science and Technology (2013CB933801, 2012AA062903) and NNSFC (21390400, 21172228, 21101163, 21273259, 21301182, 81171633).

Notes and references

[a] *Key Laboratory of Photochemical Conversion and Optoelectronic Materials, Technical Institute of Physics and Chemistry, Chinese Academy of Sciences, Beijing 100190, P. R. China; E-mail: xswang@mail.ipc.ac.cn and zhouqianxiong@mail.ipc.ac.cn*

[b] *Graduate School of Chinese Academy of Sciences, Beijing 100049, P. R. China.*

† Electronic Supplementary Information (ESI) available: Crystal data and structure refinement parameters of **2**, absorption and emission spectra changes of **1-3** in PBS or CH_3CN in the dark or upon irradiation at λ > 400 or 550 nm in the absence or presence of DABCO or NaN_3, high-resolution ESI MS and ^{1}H NMR spectra of **1-3** before and after irradiation, DNA electrophoresis in varied conditions, confocal micrographs of A549 cells with Hoechst 34580 and **1.** See DOI: 10.1039/b000000x/

1 (a) N. P. E. Barry and P. J. Sadler, *Chem Commun.,* 2013, **49**, 5106-5131; (b) T. Gianferrara, I. Bratsos and E. Alessio, *Dalton Trans*., 2009, 7588-7598; (c) I. Ojima, *Acc. Chem. Res.,* 2008, **41**, 108-119.

2 (a) P. Rai, S. Mallidi, X. Zheng, R. Rahmanzadeh, Y. Mir, S. Elrington, A. Khurshid and T. Hasan, *Adv. Drug Delivery Rev.,* 2010, **62**, 1094-1124; (b) J. P. Celli, B. Q. Spring, I. Rizvi, C. L. Evans, K. S. Samkoe, S. Verma, B. W. Pogue and T. Hasan, *Chem. Rev.,* 2010, **110**, 2795-2838; (c) D. Crespy, K. Landfester, U. S. Schubert and A. Schiller, *Chem. Commun.,* 2010, **46**, 6651-6662.

3 (a) A. E. O'Connor, W. M. Gallagher and A. T. Byrne, *Photochem. Photobiol.*, 2009, **85**, 1053-1074; (b) M. R. Detty, S. L. Gibson and S. J. Wagner, *J. Med. Chem.*, 2004, **47**,3897-3915.

4 (a) M. C. DeRosa and R. J. Crutchley, *Coord. Chem. Rev.*, 2002, **233-234**, 351-371; (b) A. L. Harris, *Nat. Rev. Cancer*, 2002, **2**, 38-47.

5 (a) M. A. Sgambellone, A. David, R. N. Garner, K. R. Dunbar and C. Turro, *J. Am. Chem. Soc.,* 2013, **135**, 11274-11282; (b) B. S. Howerton, D. K. Heidary and E. C. Glazer, *J. Am. Chem. Soc.*, 2012, **134**, 8324-8327; (c) E. Wachter, D. K. Heidary, B. S. Howerton, S. Parkin and E. C. Glazer, *Chem. Commun.,* 2012, **48**, 9649-9651; (d) R. E. Goldbach, I. Rodriguez-Garcia, J. H. van Lenthe, M. A. Siegler and S. Bonnet, *Chem. Eur. J.*, 2011, **17**, 9924-9929; (e) S. J. Berners-Price, *Angew. Chem. Int. Ed.*, 2011, **50**, 804-805; (f) N. J. Farrer, J. A. Woods, L. Salassa, Y. Zhao, K. S. Robinson, G. Clarkson, F. S. Mackay and P. J. Sadler, *Angew. Chem. Int. Ed*., 2010, **49**, 8905 -8908; (g) N. J. Farrer, L. Salassa and P. J. Sadler, *Dalton Trans.*, 2009, 10690-10701; (h) F. S. Mackay, J. A. Woods, P. Heringová, J. Kašpárková, A. M. Pizarro, S. A. Moggach, S. Parsons, V. Brabec and P. J. Sadler, *PNAS,* 2007, **104**, 20743-20748.

6 (a) J. Suryadi and U. Bierbach, *Chem. Eur. J.*, 2012, **18**, 12926-12934. (b) Ž. D. Bugarčić, J. Bogojeski, B. Petrović, S. Hochreuther and R. Eldik, *Dalton Trans.*, 2012, **41**, 12329-12345.

7 (a) G. S. Smith and B. Therrien, *Dalton Trans.*, 2011, **40**, 10793-10800; (b) P. J. Dyson and G. Sava, *Dalton Trans.*, 2006, 1929-1933; (c) Y. K. Yan, M. Melchart, A. Habtemariam and P. J. Sadler, *Chem. Commun.*, 2005, 4764-4776.

8 (a) Q. X. Zhou, W. H. Lei, Y. J. Hou, Y. J. Chen, C. Li, B. W. Zhang and X. S. Wang, *Dalton Trans.*, 2013, **42**, 2786-2791; (b) S . Betanzos-Lara, L. Salassa, A. Habtemariam, O. Novakova, A. M. Pizarro, G. J. Clarkson, B. Liskova, V. Brabec and P. J. Sadler, *Organometallics,* 2012, **31**, 3466-3479; (c) S. Betanzos-Lara, L. Salassa, A. Habtemariam and P. J. Sadler, *Chem. Commun.,* 2009, 6622-6624.

9 (a) F. Schmitt, N. P. E. Barry, L. Juillerat-Jeanneret and B. Therrien, *Bioorg. Med. Chem. Lett.,* 2012, **22**, 178-180; (b) M. Pernot, T. Bastogne, N. P. E. Barry, B. Therrien, G. Koellensperger, S. Hann, V. Reshetov and M. Barberi-Heyob, *J. Photochem. Photobiol. B, Biol.,* 2012, **117**, 80-89; (c) F. Schmitt, P. Govindaswamy, O. Zava, G. Süss-Fink, L. Juillerat-Jeanneret and B. Therrien, *J. Biol. Inorg. Chem.,* 2009, **14**, 101-109; (d) F. Schmitt, P. Govindaswamy, G. Süss-Fink, W. H. Ang, P. J. Dyson, L. Juillerat-Jeanneret and B. Therrien, *J. Med. Chem.,* 2008, **51**, 1811-1816.

10 T. Gianferrara, A. Bergamo, I. Bratsos, B. Milani, C. Spagnul, G. Sava and E. Alessio, *J. Med. Chem.,* 2010, **53**, 4678-4690; (b) T. Gianferrara, I. Bratsos, E. Iengo, B. Milani, A. Oštrić, C. Spagnul, E. Zangrando and E. Alessio, *Dalton Trans.*, 2009, 10742-10756.

11 (a) P. Sweigert, Z. Xu, Y. Hong and S. Swavey, *Dalton Trans.,* 2012, **41**, 5201-5208; (b) Z. Xu and S. Swavey, *Dalton Trans.*, 2011, **40**, 7319-7326; (c) M. Cunningham, A. McCrate, M. Nielsen and S. Swavey, *Eur. J. Inorg. Chem.,* 2009, 1521-1525; (d) S. Rani-Beeram, K. Meyer, A. McCrate, Y. Hong, M. Nielsen and S. Swavey, *Inorg. Chem.,* 2008, **47**, 11278-11283.

12 (a) T. Stuchinskaya, M. Moreno, M. J. Cook, D. R. Edwards and D. A. Russell, *Photochem. Photobiol. Sci.,* 2011, **10**, 822-831; (b) E. F. F. Silva, C. Serpa, J. M. Dabrowski, C. J. P. Monteiro, S. J. Formosinho, G. Stochel, K. Urbanska, S. Simoes, M. M. Pereira and L. G. Arnaut, *Chem. Eur. J.,* 2010, **16**, 9273-9286.

13 (a) R. L. Williams, H. N. Toft, B. Winkel and K. J. Brewer, *Inorg. Chem.*, 2003, **42**, 4394-4400; (b) M. Milkevitch, B. W. Shirley and K. J. Brewer, *Inorg. Chim. Acta.*, 1997, **264**, 249-256; (c) M. Milkevitch, H. Storrie, E. Brauns, K. J. Brewer and B. W. Shirley, *Inorg. Chem.*, 1997, **36**, 4534-4538; (d) Y. Y. Ng, C. M. Che and S. M. Peng, *New J. Chem.*, 1996, **20**, 781.

14 (a) Q. X. Zhou, W. H. Lei, Y. Sun, J. R. Chen, C. Li, Y. J. Hou, X. S. Wang and B. W. Zhang, *Inorg. Chem.*, 2010, **49**, 4729-4731; (b) Q. X. Zhou, W. H. Lei, J. R. Chen, C. Li, Y. J. Hou, X. S. Wang and B. W. Zhang, *Chem. Eur. J.*, 2010, **16**, 3157-3165.

15 (a) J. Wang, J. Newman Jr., S. L. H. Higgins, K. M. Brewer, B. S. J. Winkel and K. J. Brewer, *Angew. Chem. Int. Ed.*, 2013, **52**, 1262-

1265; (b) S. L. H. Higgins, A. J. Tucker, B. S. J. Winkel and K. J. Brewer, *Chem. Commun.,* 2012, **48**, 67-79; (c) S. L. H. Higgins, T. A. White, B. S. J. Winkel and K. J. Brewer, *Inorg. Chem.,* 2011, **50**, 463-470; (d) R. Miao, M. T. Mongelli, D. F. Zigler, B. S. J. Winkel and K. J. Brewer, *Inorg. Chem.,* 2006, **45**, 10413-10415.

16 B. A. Albani, B. Peña, K. R. Dunbar and C. Turro, *Photochem. Photobiol.Sci.,* 2014, **13**, 272-280.

17 Q. X. Zhou, W. H. Lei, Y. J. Chen, C. Li, Y. J. Hou, B. W. Zhang and X. S. Wang, *Chem. Eur. J.,* 2012, **18**, 8617-8621.

18 (a) T. Bugarcic, A. Habtemariam, J. Stepankova, P. Heringova, J. Kasparkova, R. J. Deeth, R. D. L. Johnstone, A. Prescimone, A. Parkin, S. Parsons, V. Brabec and P. J. Sadler, *Inorg. Chem.,* 2008, **47**, 11470-11486; (b) S. W. Magennis, A. Habtemariam, O. Novakova, J. B. Henry, S. Meier, S. Parsons, I. D. H. Oswald, V. Brabec and P. J. Sadler, *Inorg. Chem.,* 2007, **46**, 5059-5068; (c) R. Lalrempuia and M. R. Kollipara, *Polyhedron*, 2003, **22**, 3155-3160.

19 (a) C. Hadjur, A. Jeunet and P. J. Jardon, *Photochem. Photobiol. B,* 1994, **26**, 67-74; (b) Y. Lion, M. Delmelle and A. Van De Vorst, *Nature,* 1976, **263**, 442-443.

20 Y. Li and M. A. Trush, *Cancer Res.,* 1994, **54**, 1895.

21 A. A. Abdel-Shafi, P. D. Beer, R. J. Mortimer and F. Wilkinson, *J. Phys. Chem. A,* 2000, **104**, 192-202.

22 R. H. Young, K. Wehrly and R. L. Martin, *J. Am. Chem. Soc.,* 1971, **93**, 5774-5779.

23 H. A. Goodwin and F. Lions, *J. Am. Chem. Soc.,* 1959, **81**, 6415-6422.

Table of Contents

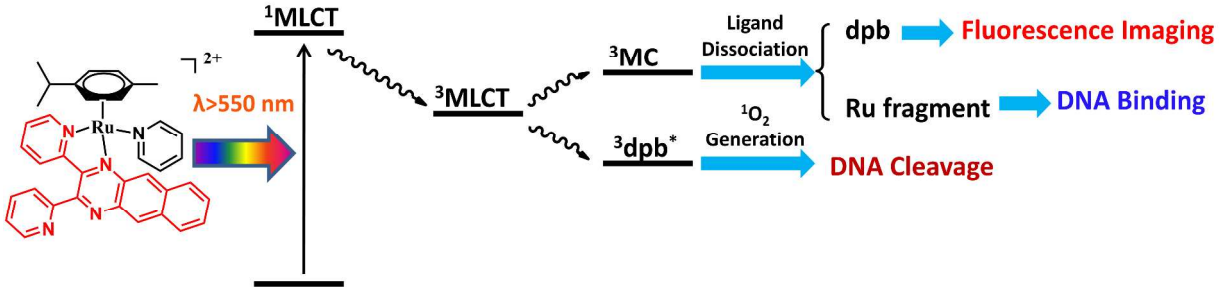

A Ru(II) arene complex displays DNA binding, DNA cleavage, and fluorescence imaging upon visible light illumination at λ > 550 nm due to the use of dpb as a bidentate ligand.